Journal of
MATERIALS RESEARCH

Substrate effects on nanoindentation mechanical property measurement of soft films on hard substrates

T. Y. Tsui and G. M. Pharr
Department of Materials Science, Rice University, 6100 Main Street; MS 321, Houston, Texas 77251-1892

(Received 20 October 1997; accepted 15 March 1998)

Substrate effects on the measurement of thin film mechanical properties by nanoindentation methods have been studied experimentally using a model soft film on hard substrate system: aluminum on glass. The hardness and elastic modulus of aluminum films with thicknesses of 240, 650, and 1700 nm sputter-deposited on glass were systematically characterized as a function of indenter penetration depth using standard nanoindentation methods. Scanning electron and atomic force microscopy of the hardness impressions revealed that indentation pileup in the aluminum is significantly enhanced by the substrate. The substrate also affects the form of the unloading curve in a manner that has important implications for nanoindentation data analysis procedures. Because of these effects, nanoindentation measurement techniques overestimate the film hardness and elastic modulus by as much as 100% and 50%, respectively, depending on the indentation depth. The largest errors occur at depths approximately equal to the film thickness.

I. INTRODUCTION

Nanoindentation is a widely used technique for measuring mechanical properties at very small length scales.[1–12] With good equipment and experimental technique, properties such as hardness and elastic modulus can be measured from indentation contacts as shallow as 20 nm.[9,10,12] The lateral resolution of the technique depends on the geometry of the indenter; for the frequently used Berkovich triangular pyramid, the lateral dimension of the contact impression is approximately seven times the depth, so meaningful measurements are possible for contact impressions with lateral dimensions of about 0.1 μm. The ability to probe at such fine scales has made nanoindentation one of the premier tools for characterizing the mechanical properties of thin films. Another advantage of nanoindentation in thin film studies is that properties can often be measured without having to remove the film from its substrate.

Standard methods for deriving properties from nanoindentation load-displacement data have been developed primarily for monolithic materials.[8,9,11] Nevertheless, these same methods are frequently applied to thin film systems without explicit consideration of how the substrate influences the measurements.[10,13,14] One approach for dealing with substrate influences is to make the indentations small enough to avoid substrate effects altogether, which is accomplished in practice by constraining the indentation depth to a small fraction of the film thickness. A commonly used rule of thumb suggests that substrate independent measurements can be obtained if the indentation depth is kept to less than one-tenth the film thickness. While experimentally feasible for films that are greater than about a micron thick, this approach cannot be used for very thin films. For example, according to the rule, nanoindentation characterization of a 0.1 μm film typical of current semiconductor technology would have to be made at a penetration depth of less than 10 nm. Since accurate measurements at this scale are difficult to obtain due to vibration, uncertainties in indenter tip geometry, and difficulties in precise determination of the location of the specimen surface, other methods for dealing with substrate influences must be developed if nanoindentation techniques are to be useful in the mechanical characterization of very thin films.

In this paper, the influences that a hard substrate exerts on the nanoindentation measurement of the hardness, H, and elastic modulus, E, of a soft film are examined for a model system: aluminum on glass. Soft films on hard substrates are quite common in the semiconductor industry, where aluminum, copper, and gold are often deposited on silicon ($H = 12$ GPa), germanium ($H = 10$ GPa), glass ($H = 5$–8 GPa), and hard ceramics ($H = 10$–40 GPa). Since the hardness of these thin metal films is usually in the range 0.1–1 GPa, the films are at least an order of magnitude softer than the materials on which they are deposited. One important consequence is that when an indentation is made in the film, material piles up around the hardness impression to a much greater degree than it would in a monolithic material due to the severe constraint imposed on plasticity in the film by the relatively undeformable substrate. Since current techniques for deriving mechanical properties from nanoindentation load-displacement data do not account for the extra contact area produced by the pileup,[15–18] substrate-induced enhancement of

 © 1999 Materials Research Society

pileup has important consequences for film property measurement accuracy. Important insights gained from experimental observations of the model aluminum/glass system and their implications for mechanical property measurement by nanoindentation methods are presented and discussed.

II. EXPERIMENTAL

A. Specimen materials

The model system used in the investigation was high purity aluminum sputter-deposited onto silicate glass substrates. In addition to a large difference in hardness (the film hardness is in the range 0.5–1.0 GPa while that for the substrate is about 7.0 GPa as determined by direct measurement), an equally important consideration in the choice of this system was the similarity of the elastic moduli of the two components. The modulus of bulk aluminum is 70 GPa while that for the glass used in the study was 57 GPa (as measured by nanoindentation techniques). The fact that the moduli are similar minimizes the role that a film/substrate modulus difference would play in the indentation behavior, thus simplifying the interpretation of results. As a result, the current work focuses on differences in the plastic behavior of the film and substrate. Influences of differences of the elastic properties of the film and substrate have been addressed from a theoretical perspective in several other studies.[13,19,20]

Three different films with thicknesses of 240 nm, 650 nm, and 1700 nm were investigated. The thinnest film (240 nm) was used primarily to explore indentation completely through the film into the substrate, the thickest film (1700 nm) for indentation entirely within the film, and the intermediate film (650 nm) for cases in between.

B. Procedures

Nanoindentation tests were conducted using a Berkovich diamond indenter with a shape function calibrated using procedures described elsewhere.[9] Indentations were made to a variety of peak loads using a five part indentation procedure. After surface contact was detected, the indenter was (1) loaded at constant loading rate at a rate chosen to reach the target peak load in 10 s; (2) held at the peak load for 10 s; (3) unloaded to 85% of the peak load at half the rate used during loading (halving the rate was employed to increase the number of data points in the unloading curve and better define the unloading behavior); (4) held at 85% of the peak load for 100 s; and (5) completely unloaded at the same rate used in step (3). Peak loads were chosen so that penetration depths varied from 0.1 to 10 times the film thickness. Data obtained in the 100 s load hold period were used to correct the displacement data for thermal drift.

Following indentation, the hardness impressions were imaged using high resolution scanning electron microscopy (SEM) and atomic force microscopy (AFM) to measure contact areas and carefully examine the extent and nature of pileup. Two different contact areas were determined from the SEM images. As shown in Fig. 1(a), the corner-to-corner area, A_{cc}, was measured from the area of the triangle defined by the corners of the hardness impression. Provided that pileup is minimal at the impression corners, the corner-to-corner area is a direct measure of the contact area that would have occurred if the film did not pile up. No significant pileup at indentation corners was observed for any of the hardness impressions in this study, as is evident in

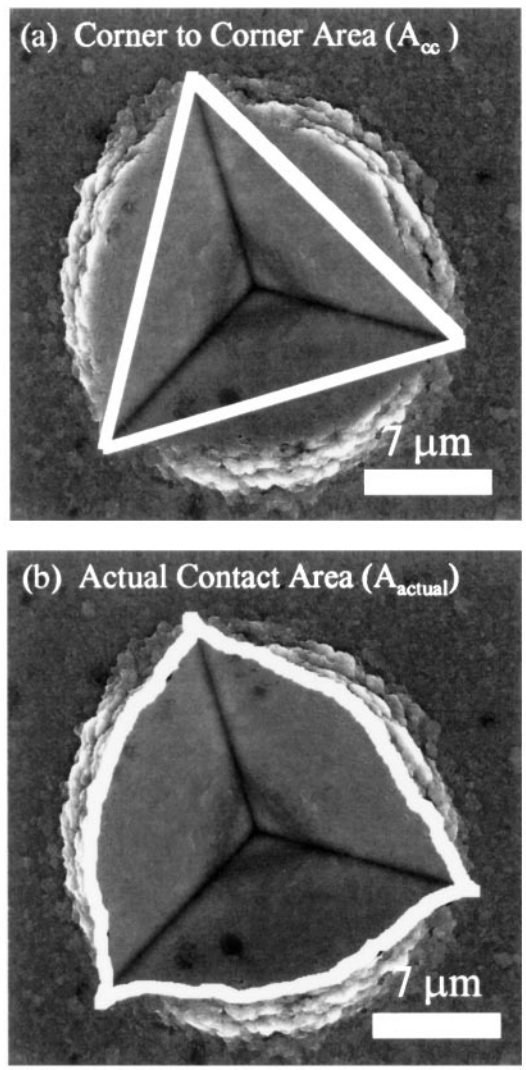

FIG. 1. Scanning electron micrographs of an indentation in the 1700 nm aluminum film illustrating the difference between (a) the corner-to-corner area, A_{cc}; and (b) the actual area including the pile-up, A_{actual}.

the SEM micrographs in Fig. 1 and was verified by AFM measurements. The second measure of the contact area was the actual contact area, A_{actual}, which includes the extra area contained in the pileup. In general, the actual contact areas were considerably larger than the corner-to-corner areas due to the bowed-out indentation edges caused by pileup. Actual contact areas were measured by tracing a digital image of the indentation along the contact edges and computing the area enclosed in the figure. The contact edge of the indentation in Fig. 1(a) is traced in Fig. 1(b). One reason for defining these two separate measures of the contact area is that their ratio, $A_{\text{actual}}/A_{\text{cc}}$, provides a convenient measure of the amount of pileup; pileup occurs when this area ratio is greater than one, and the amount of pileup increases with the ratio. Values of $A_{\text{actual}}/A_{\text{cc}}$ less than one, which indicate sink-in behavior, were not observed for any indentation in this study.

C. Data analysis

The indentation load-displacement data obtained at each depth were analyzed to determine the hardness, H, and elastic modulus, E, using the method of Oliver and Pharr.[9] In this method, the hardness and modulus are determined from the relations:

$$H = \frac{P_{\max}}{A} \tag{1}$$

and

$$E = (1 - \nu^2)\left[\frac{2}{\sqrt{\pi}}\beta\frac{\sqrt{A}}{S} - \frac{1 - \nu_i^2}{E_i}\right]^{-1}, \tag{2}$$

where $P_{\max}$ is the peak indentation load, A is the indentation contact area, β is a constant which depends on the indenter geometry, S is the experimentally measured contact stiffness, ν is Poisson's ratio for the specimen, and ν_i and E_i are Poisson's ratio and the elastic modulus of the indenter. For the Berkovich diamond used in all experiments, $\beta = 1.034$, $\nu_i = 0.07$, and $E_i = 1141$ GPa.[9] It was assumed in all calculations that Poisson's ratio for the specimen is 0.34.

Following procedures developed by Oliver and Pharr,[9] the contact stiffness in Eq. (2) was determined by fitting the unloading data to the power-law relation

$$P = \alpha(h - h_f)^m, \tag{3}$$

and numerically evaluating the derivative of the curve fit at the maximum indentation depth. In Eq. (3), P is the indentation load, h is the indenter displacement, h_f is the final indentation depth, and α and m are fitting parameters. In most stiffness evaluations, the upper 90% of the first unloading segment was used to determine the curve fitting parameters. Recall that the first unloading extended from peak load to 15% of the peak load.

The other quantity needed to evaluate the hardness and elastic modulus by means of Eqs. (1) and (2) is the contact area, A. In the Oliver–Pharr method, the contact area is determined by evaluating the indenter shape function at the contact depth, h_c, where the contact depth is estimated from the indentation load-displacement data by a procedure based on a solution for the indentation of an elastic half-space by a rigid punch. Because the analysis is strictly elastic, this procedure inherently ignores contributions to the contact area due to plasticity and pileup, and thus leads to an underestimation of the contact area and a corresponding overestimation of the hardness and elastic modulus [see Eqs. (1) and (2)].[16–18] For this reason, H and E were evaluated in this work using two separate measures of the contact area: (1) A_{nano}, the area determined by applying the Oliver–Pharr analysis procedure to the experimental load-displacement data, and (2) A_{actual}, the actual contact area measured from SEM micrographs like that in Fig. 1(b). Comparison of these two areas provides important insight as to when and why nanoindentation film property measurements may be inaccurate.

III. RESULTS AND DISCUSSION

Throughout this work, results will be presented as a function of the maximum indentation depth, $h_{\max}$, normalized with respect to the film thickness, t_f. This normalization is chosen to allow for direct comparison of data for films of different thickness. Since the pyramidal geometry of the Berkovich indenter is self-similar, the only linear scaling factor in the indentation process is the film thickness, and results for films of differing thickness must scale with $h_{\max}/t_f$. The parameter $h_{\max}$ is chosen in preference to the contact depth, h_c, since determination of the contact depth from indentation load-displacement data is currently possible only for monolithic materials.[9] Moreover, accurate measurement of the contact depth from load-displacement data can be achieved only in materials which do not pile up, as has recently been shown using finite element methods.[18]

Basic nanoindentation measurements are presented in Figs. 2 and 3, where the elastic modulus and hardness of the 1700 nm aluminum film are plotted as a function of $h_{\max}/t_f$. Each data point is an average from at least 5 indentations, with error bars indicating one standard deviation. Note that the error bars in many cases are smaller than the size of the plotting symbol and thus do not appear explicitly. All data in Figs. 2 and 3 were computed from stiffnesses derived by fitting the upper 90% of the unloading curve.

The open circles in Fig. 2 are the elastic moduli determined by standard nanoindentation data analysis procedures, i.e., by using in Eq. (2) the contact area deduced from the nanoindentation load-displacement data,

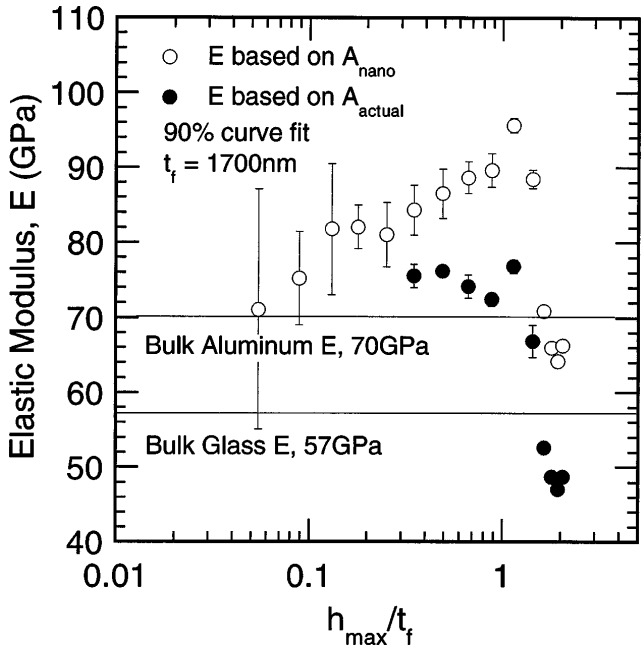

FIG. 2. Dependence of the elastic modulus of the 1700 nm film on the normalized indentation depth, $h_{\max}/t_f$. Contact stiffnesses were determined by a power law curve fit of the upper 90% of the unloading data.

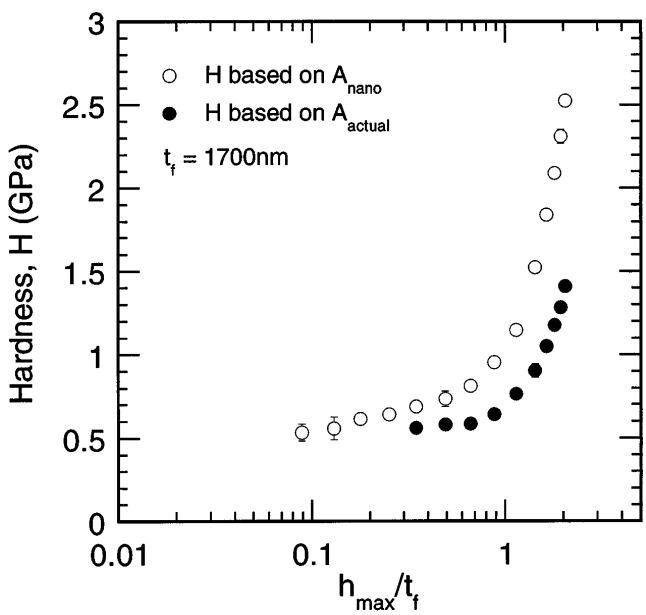

FIG. 3. Dependence of the hardness of the 1700 nm film on the normalized indentation depth, $h_{\max}/t_f$.

A_{nano}. At small depths, the nanoindentation modulus is close to the 70 GPa value for bulk aluminum. However, at larger depths there is an unexpected increase in the modulus to a peak value of about 90–100 GPa at indentation depths close to the film thickness. This increase in modulus cannot be attributed directly to the substrate, since the substrate modulus, 57 GPa, is smaller than that for bulk aluminum. As the indentation depth increases beyond the film thickness, the nanoindentation modulus drops sharply to about 65 GPa.

The nanoindentation hardness of the 1700 nm film is shown by the open circles in Fig. 3. The hardness is approximately 0.5 GPa at small depths, and increases smoothly to about 1 GPa at depths close to the film thickness. This factor of two increase in hardness for indentations within the film is similar to nanoindentation measurements of thin aluminum films on silicon substrates by Doerner, Gardener, and Nix[7] and Stone *et al.*[21] As the depth increases beyond the film thickness, the hardness increases rapidly toward the value of the glass substrate, 7.0 GPa.

Careful examination of the contact impressions in the films revealed that the higher than expected elastic moduli in Fig. 2 originate from substrate-induced enhancement of pileup. Three SEM images illustrating the nature of the pileup are shown in Fig. 4. Included with each image is an AFM trace of the surface profile along the line shown on the SEM image. Figure 4(a) is an indentation in the 1700 nm film at a depth much less than the film thickness, i.e., $h_{\max} \ll t_f$. Figures 4(b) and 4(c) show indentations in the 240 nm film for which $h_{\max} \approx t_f$ [Fig. 4(b)] and $h_{\max} \gg t_f$ [Fig. 4(c)]. Pileup of vari-

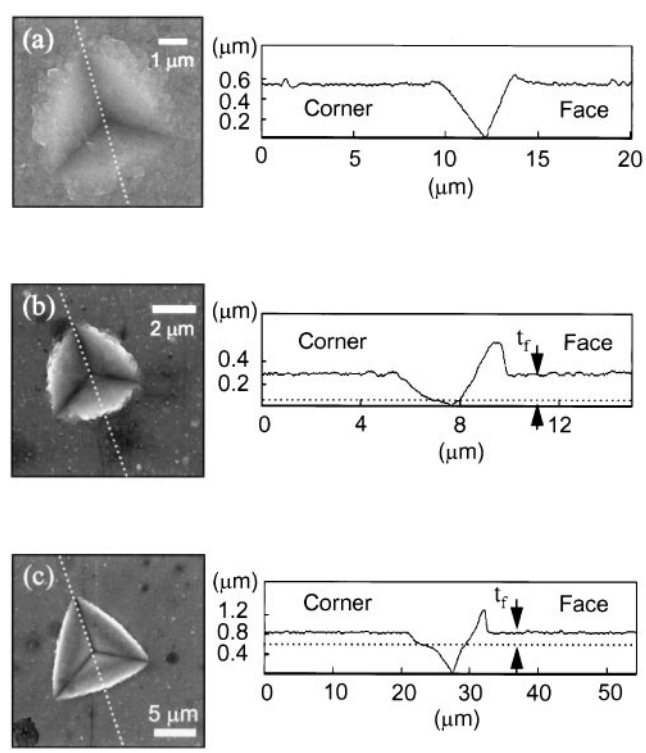

FIG. 4. Scanning electron micrographs and atomic force microscope surface profile traces for three indentations: (a) 1700 nm film, $h_{\max} \ll t_f$; (b) 240 nm film, $h_{\max} \approx t_f$; (c) 240 nm film; $h_{\max} \gg t_f$. The AFM traces were made along the lines shown in the SEM micrographs.

ous forms is clearly visible in all three SEM images. One notable feature is the nonuniform distribution of pileup around the contact periphery; pileup is most extensive near the centers of the edges of the indentation but virtually absent at the corners, as verified by the AFM surface profiles. The AFM traces also show that the height of the pileup relative to the total penetration depth is greatest for the indentation for which $h_{\max} \approx t_f$ [Fig. 4(b)]. Another notable feature is the change in the shape of the contact geometry at the contact periphery from triangular at small depths [Fig. 4(a)] to roughly circular at the contact depths close to the film thickness [Fig. 4(b)] and then to triangular again at larger depths [Fig. 4(c)]. These changes are due to differences in the form and distribution of the pileup in each of the three cases.

In order to further examine the structure of the pileup, an indentation in the 1700 nm film was cross-sectioned using a focused-ion-beam technique and imaged in the SEM. Figures 5(a) and 5(b) show cross sections in two different orientations indicated by the insets. It is evident that the film remains fully adhered after indentation; i.e., there is no evidence of delamination in the vicinity of the hardness impression. The grain structure of the film is also visible, revealing flattening of grains beneath the contact impression.

From AFM profiles like those in Fig. 4, the pileup heights at the centers of the faces of the indentations, h_{pu}, were determined to provide a quantitative measure of the amount of pileup. The dependence of $h_{\mathrm{pu}}/h_{\max}$ on $h_{\max}/t_f$ is shown in Fig. 6. The parameter $A_{\mathrm{actual}}/A_{\mathrm{cc}}$, which also provides also a useful measure of the pileup (as discussed earlier), is plotted as a function of $h_{\max}/t_f$ in Fig. 7. The data in Figs. 6 and 7 reveal that the amount of pileup is relatively small at small indentation depths, in accordance with the behavior of bulk, annealed aluminum,[22] but rises to a distinct maximum at depths close to the film thickness before falling at large depths. At depths near the maximum pileup, the height of the pileup is approximately 50% of the indentation depth, and the actual contact area is about 50% greater than would be predicted based on the corner-to-corner area measurements. Apparently, as the indenter approaches

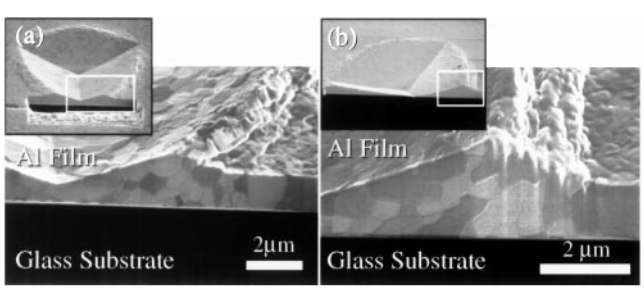

FIG. 5. (a, b) Indentation cross sections produced by focused-ion-beam techniques. Orientations of the cross sections are shown in the insets.

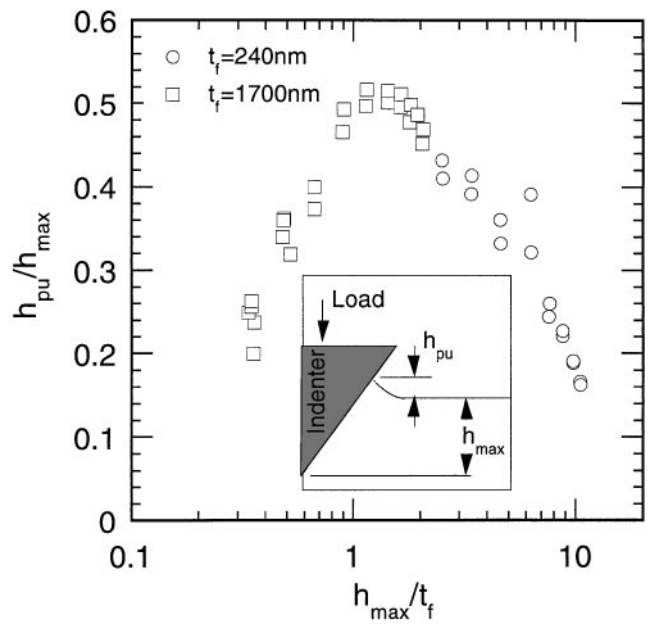

FIG. 6. Dependence of the normalized pileup height, $h_{\mathrm{pu}}/h_{\max}$, on the normalized indentation depth, $h_{\max}/t_f$.

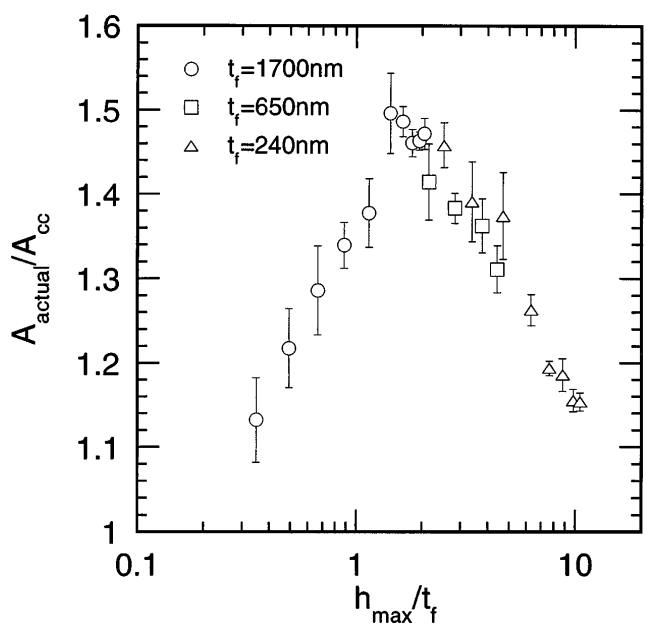

FIG. 7. Dependence of the ratio of the actual contact area to the corner-to-corner area, $A_{\mathrm{actual}}/A_{\mathrm{cc}}$, on the normalized indentation depth, $h_{\max}/t_f$.

the substrate, plastic flow in the film is restricted by the relatively nondeformable substrate in a manner that causes soft film material to flow preferentially toward the surface and enhances pileup. The relative amount of pileup decreases when the indenter penetrates through the film because there is no pileup for indentations in glass.[22] The absence of pileup at small depths suggests that the as-deposited aluminum must work-harden, since

it is well documented, both experimentally[23] and by finite element simulation,[18,24] that pileup in monolithic materials is diminished by work-hardening. On the other hand, if the film were elastic-perfectly-plastic (i.e., no work-hardening), pileup would be expected even at the smallest penetration depths, but presumably would increase with depth due to substrate constraint.

The fact that there is significant substrate-induced pileup in the aluminum films means that the contact areas deduced from the nanoindentation load-displacement data by the Oliver–Pharr method are in error, which in turn produces errors in the nanoindentation hardness and elastic modulus. To examine the extent to which this is related to the modulus observations in Fig. 2, Eq. (2) has been used to recompute the elastic moduli based on A_{actual}, the actual contact areas measured from the SEM micrographs. Results are plotted in Fig. 2 as filled circles. Note that some of the very small indentations could not be imaged with sufficient resolution to make accurate area measurements and are therefore not included in the plot. The data show that for indentation depths less than the film thickness, use of the actual contact areas reduces the measured moduli to relatively constant values in the range 72–77 GPa and thus much closer to what would be expected. On the other hand, for indentation depths greater than the film thickness, the modulus drops sharply to ~47 GPa, a value much lower than the modulus of either bulk aluminum (70 GPa) or bulk glass (57 GPa). The origin of this behavior will be discussed shortly.

The hardnesses computed from the actual contact areas are shown as filled circles in Fig. 3. Like the modulus, use of the actual contact area reduces the hardness by as much as a factor of two depending on the indentation depth. An interesting feature of this data is the relative constancy of the actual hardness for indentation depths within the film thickness. Thus, the factor of two increase observed in the nanoindentation hardnesses is not real but an artifact related to pileup. Hardness data for the 240 and 650 nm films are presented in Fig. 8 and show how even for penetration depths as large as 10 times the film thickness, the nanoindentation hardnesses overestimate the actual hardnesses by a measurable amount. Note also how the actual hardnesses increase steadily over the entire range. Apparently, much greater depths must be reached before the measured values are dominated by the substrate hardness ($H = 7.0$ GPa), and the hardness levels off in a plateau.

In order to understand the abrupt drop in modulus at depths beyond the film thickness, it is useful to begin by examining the AFM indentation contact profiles in Fig. 4. Figure 4(a) is an indentation made entirely within the film. Due to the small amount of elastic recovery in aluminum, the AFM profile has very straight edges, and the contact impression closely resembles the shape of

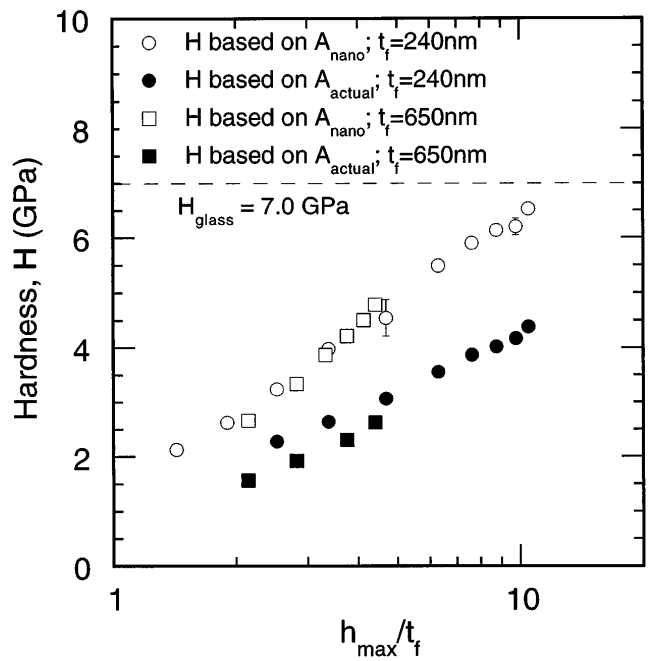

FIG. 8. Dependence of the hardness of the 240 and 650 nm films on the normalized indentation depth, $h_{\max}/t_f$.

the indenter. Figure 4(b), on the other hand, shows an indentation for which the indenter has slightly penetrated through the film ($h_{\max} \approx t_f$). While the upper portion of this impression resembles the indenter shape, near the bottom there is a distinct flattening and change in profile relative to the impression in Fig. 4(a). Figure 4(c) shows a residual impression whose depth is about three times the film thickness ($h_{\max} \gg t_f$). Again, the upper portion of the impression resembles the indenter geometry, but at the film-substrate interface, there is a transition in profile from the straight edges characteristic of indentations in aluminum to the cusp-like shape characteristic of indentations in bulk glass.[22]

It is now useful to consider what physically occurs during the unloading of an indentation that penetrates through the soft aluminum film into the hard glass substrate. First note that the elastic displacements recovered during the unloading of aluminum are much smaller than for glass. This is because the greater hardness of glass results in greater contact pressures, and since the moduli of the two materials are similar, a greater fraction of the total displacement is elastic. As a result, only about 5% of the displacement at $P_{\max}$ is elastically recovered during the unloading of aluminum, while for glass the elastic recovery is nearly 40%.[22] With this in mind, Fig. 9 shows schematically the unloading of an aluminum film on a glass substrate and a hypothetical interpretation of the indentation load-displacement behavior. When the indenter is fully loaded, Fig. 9(a), both the film and substrate are in contact with the indenter. However, after only a small amount of unloading

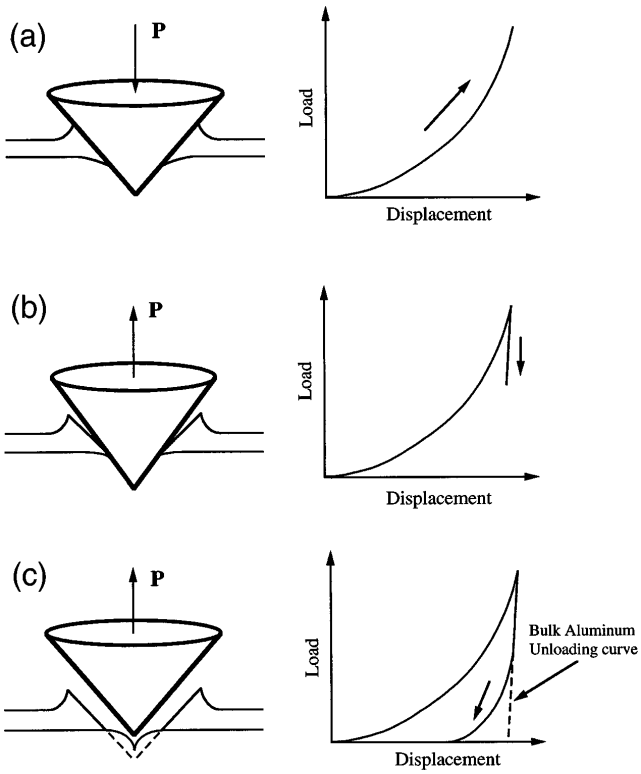

FIG. 9. (a–c) Schematic representation of the unloading process for an indentation that has penetrated through the film.

displacement, the indenter loses contact with the film due to the relatively small amount of elastic recovery in the aluminum [Fig. 9(b)], and further unloading occurs by elastic recovery in the substrate only [Fig. 9(c)]. An important consequence is that most of the unloading curve is dominated by the elastic properties of the substrate, which produces a change in the shape of the unloading curve near the point at which film contact is lost. In addition, since glass recovers to a greater degree than aluminum, the residual contact impression has a distinctly different shape at the bottom than at the top. The net result is a contact impression profile with a distinct change from straight-sided to cusp-like at the film-substrate interface, similar to that observed in the AFM profile of Fig. 4(c).

The change in shape of the unloading curve for indentations made through the film into the substrate has important consequences for the measurement of contact stiffness from the load-displacement data. To illustrate this, Figs. 10 and 11 present unloading curves for two different indentations in the 1700 nm film along with curve fits obtained by applying the power-law relation of Eq. (3) to 90% of the first unloading data. The primary difference in the two sets of data is the depth of penetration; in Fig. 10, the indentation resides entirely within the film ($h_{\max} = 590$ nm; $h_f = 560$ nm), whereas in Fig. 11, the indenter penetrated through the film ($h_{\max} =$

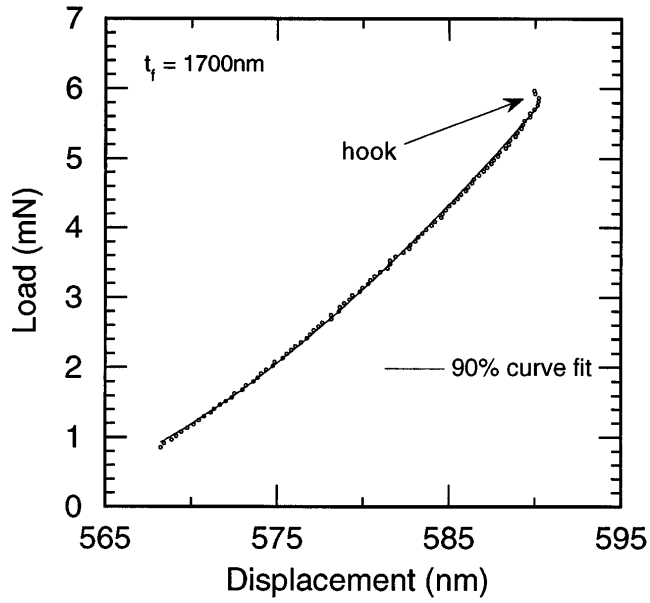

FIG. 10. Load-displacement data during unloading for an indentation with a depth less than the film thickness (1700 nm film).

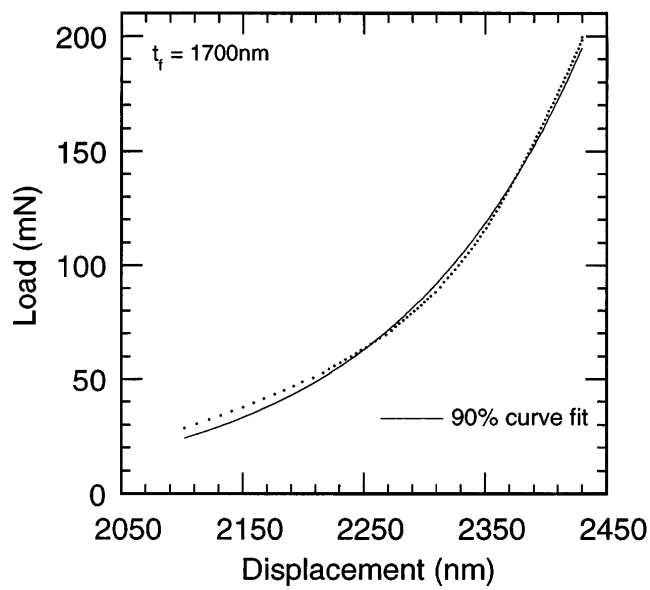

FIG. 11. Load-displacement data during unloading for an indentation with a depth greater than the film thickness (1700 nm film).

2430 nm; $h_f = 1940$ nm). With the exception of the small "hook" at the top of the data, the 90% power law fit provides a reasonable approximation of the data in Fig. 10. Implications of the "hook," which is due to creep in the aluminum, will be discussed shortly. On the other hand, the power law fit is not nearly so good for the data in Fig. 11 due to the bend in the lower part of the data caused by elastic recovery of the substrate. In particular, the fit noticeably underestimates the slope of the upper portion of the data and therefore the contact

stiffness from which the elastic modulus is derived by means of Eq. (2).

To explore what effect this has on nanoindentation elastic modulus measurement, the data in Fig. 2 were recomputed using only the upper 50% of the unloading curve for the power law curve fitting. Results are plotted in Fig. 12. For monolithic materials, there is usually less than a 2% difference in the elastic moduli determined using 90% and 50% curve fits.[22] However, comparison of results in Figs. 2 and 11 shows that this is not the case for aluminum films on glass. As expected, reducing the portion of the data used in the curve fit increases the measured moduli. At depths greater than the film thickness, the moduli computed from the actual contact areas increase from 47–50 GPa (Fig. 2) to 60–70 GPa (Fig. 12) and are thus in reasonable agreement with what would be expected based on the known moduli of the glass (57 GPa) and aluminum (70 GPa). Curiously, however, the moduli for indentation depths less than the film thickness are also increased, some to as high as 92 GPa.

A complete understanding as to why the elastic moduli at indentation depths less than the film thickness are higher than expected for the 50% curve fits has not yet been established. One possibility is that Eq. (2) does not rigorously apply to film-on-substrate systems, even when the elastic moduli of the two materials are approximately the same, since the equation is derived from an analysis that assumes monolithic material behavior and ignores plasticity. Another possibility is that the high moduli are an experimental artifact due to creep deformation in the aluminum film. Indentations in aluminum may exhibit time-dependent creep deformation, which manifests itself as a "hook" in the upper portion of the unloading data like that shown in Fig. 9. In the current experiments, creep displacement rates large enough to measurably affect the unloading stiffnesses were observed in the 10-s peak load constant load hold period just prior to unloading. Creep has the effect of artificially increasing the apparent contact stiffness, with the artifact being more pronounced when smaller portions of the unloading data are used in curve-fitting procedures. Thus, if the amount of creep in the aluminum films is large, the data in Fig. 2 (90% fit) rather than that in Fig. 10 (50% fit) would provide a better estimate of the elastic modulus for indentations made within the film. Unfortunately, exactly how much of the difference in the moduli in Figs. 2 and 12 is due to creep cannot be unambiguously assessed due to uncertainties in removing the time-dependent portion of the indenter displacement from the unloading data. However, recent finite element simulations of conical indentation of aluminum films on glass, in which creep effects can be avoided through the choice of constitutive behavior, have shown that Eq. (2) works well for film/substrate systems in which the moduli are matched, thus suggesting that the overestimation of the modulus in the present work is more likely due to creep.[25]

Lastly, it is instructive to examine how the hardness measurements are influenced by the relative amount of the unloading data used in curve fitting procedures. Figure 13, which shows hardnesses determined from both 90% and 50% curve fits, demonstrates that the nanoindentation hardness is not nearly so strongly af-

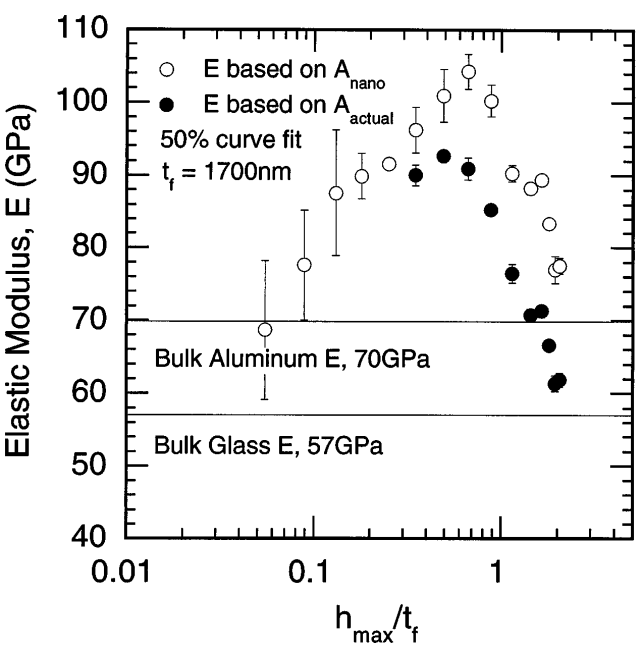

FIG. 12. Dependence of the elastic modulus of the 1700 nm film on the normalized indentation depth, h_{max}/t_f. Contact stiffnesses were determined by a power law curve fit of the upper 50% of the unloading data.

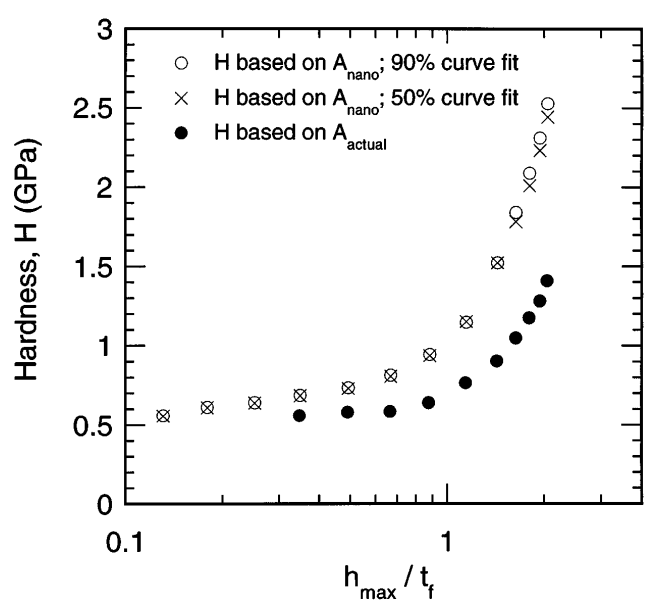

FIG. 13. Dependence of the hardness of the 1700 nm film on the normalized indentation depth, h_{max}/t_f, illustrating the small differences obtained using 50 and 90% curve fits of the unloading data.

fected as the modulus results in Figs. 2 and 12. The relative insensitivity of the hardness to the fitting procedures results from the fact that, unlike the modulus, the hardness does not depend explicitly on the contact stiffness [see Eq. (1)], and is influenced by the contact stiffness only through a relatively mild effect on the experimentally measured contact depth, h_c.

IV. REMARKS

Results presented in this work show that the potential for error in the measurement of the hardness and elastic modulus of soft films on hard substrates by nanoindentation methods is significant. Errors are caused by two different effects: (1) substrate-induced enhancement of pileup, and (2) uncertainties in experimentally measured contact stiffnesses due to substrate effects on the shape of the unloading curve and creep in the film. The latter problem can be diminished and possibly eliminated by careful experimental technique and data analysis procedures. For example, the incorporation of very long peak load hold periods prior to unloading could be used to reduce the creep displacements to small levels, in which case the curve fit can be applied to smaller portions of the unloading data to obtain more accurate contact stiffnesses. Determination of the contact stiffness by continuous stiffness measurement techniques could also prove useful.[9] On the other hand, the errors caused by substrate-enhanced pileup are not so easily overcome. An effective methodology for dealing with pileup has not yet been developed, even for monolithic materials, and until one has, nanoindentation hardness and elastic modulus measurements of soft films on hard substrates must be interpreted with caution.

The data in Figs. 2, 3, 8, 12, and 13 provide some insight into how great the measurement errors may be and under what conditions the errors are large and small. In general, nanoindentation techniques can be expected to overestimate both the hardness and the elastic modulus of soft films on hard substrates, with the errors being greatest at indentation depths close to the film thickness. The overestimation can be as large as 50% for the modulus, and as large as 100% for the hardness. On the other hand, it appears that reasonable film properties can be obtained at small penetration depths. Curiously, the data in the figures show that when $h_{\max}/t_f \cong 0.1$, the nanoindentation hardness and modulus are within about 10% of the actual values, thus suggesting that there may indeed be some merit to the rule of thumb that substrate-independent measurements can be obtained when the indentation depth is less than 10% of the film thickness.

Lastly, although the results presented here are specific to one material system—aluminum on glass—many of the phenomena observed in this system undoubtedly occur in other systems in which the substrate is considerably harder than the film. Systems that behave in a similar manner can possibly be identified by the ratio of the substrate to film hardness. Since this ratio is about 10 for the aluminum/glass system, a conservative estimate is that significant substrate-induced pileup influences on nanoindentation mechanical property measurement can be expected when the substrate is at least ten times harder than the film. This observation is corroborated by recent finite element simulations of the aluminum/glass system.[25]

V. CONCLUSIONS

Indentation pileup in soft aluminum films is significantly enhanced when the films are deposited on hard substrates. Substrate-induced enhancement of pileup increases the indentation contact area by as much as 50% above what is observed in monolithic aluminum, and is greatest at indentation penetration depths close to the film thickness. Because standard methods for measuring mechanical properties by nanoindentation methods do not account for pileup, the contact area is underestimated; this produces errors in the measured hardness and elastic modulus. Additional errors are produced by inaccuracies in the measurement of contact stiffness caused by substrate effects on the shape of the unloading curve and creep in the film. Collectively, the errors result in an overestimation of the hardness by as much as 100%, and the elastic modulus by as much as 50%. When the indentation depth is about one tenth the film thickness, substrate induced enhancement of pileup is negligible, and the hardness and modulus measured by nanoindentation techniques are within 10% of the expected values.

ACKNOWLEDGMENTS

This work was supported by the Division of Materials Sciences, United States Department of Energy, under Contract DE-AC05-96OR22464 with Lockheed Martin Energy Research Corporation, and through the SHaRE Program under Contract DE-AC05-76OR00033 with Oak Ridge Associated Universities.

REFERENCES

1. T. Y. Tsui, W. C. Oliver, and G. M. Pharr, in *Thin Films: Stresses and Mechanical Properties VI,* edited by W. W. Gerberich, H. Gao, J-E. Sundgren, and S. P. Baker (Mater. Res. Soc. Symp. Proc. **436**, Pittsburgh, PA, 1997), p. 207.
2. W. C. Oliver, C. J. McHargue, and S. J. Zinkle, Thin Sol. Films **153**, 185 (1987).
3. W. C. Oliver and C. J. McHargue, Thin Sol. Films **161**, 117 (1988).
4. W. C. Oliver, R. Hutchings, and J. B. Pethica, in *Microindentation Techniques in Materials Science and Engineering,* edited by P. J. Blau and B. R. Lawn (American Society for Testing and Materials, Philadelphia, PA, 1986), pp. 90–108.

5. S. M. Gorbatkin, R. L. Rhodes, T. Y. Tsui, and W. C. Oliver, Appl. Phys. Lett. **65**, 2672 (1994).
6. B. D. Fabes and W. C. Oliver, in *Thin Films: Stresses and Mechanical Properties II,* edited by M. Doerner, W. C. Oliver, G. M. Pharr, and F. R. Brotzen (Mater. Res. Soc. Symp. Proc. **188**, Pittsburgh, PA, 1990), p. 127.
7. M. F. Doerner, D. S. Gardner, and W. D. Nix, J. Mater. Res. **1**, 845 (1986).
8. M. F. Doerner and W. D. Nix, J. Mater. Res. **1**, 601 (1986).
9. W. C. Oliver and G. M. Pharr, J. Mater. Res. **7**, 1564 (1992).
10. G. M. Pharr and W. C. Oliver, MRS Bulletin **17**, 28 (1992).
11. J. L. Loubet, J. M. Georges, O. Marchesini, and G. Meille, J. Tribology **106**, 43 (1984).
12. J. B. Pethica, R. Hutchings, and W. C. Oliver, Philos. Mag. A **48**, 593 (1983).
13. A. K. Bhattacharya and W. D. Nix, Int. J. Solids Struct. **24**, 1287 (1988).
14. T. A. Laursen and J. C. Simo, J. Mater. Res. **7**, 618 (1992).
15. T. Y. Tsui, W. C. Oliver, and G. M. Pharr, J. Mater. Res. **11**, 752 (1996).
16. A. Bolshakov, W. C. Oliver, and G. M. Pharr, J. Mater. Res. **11**, 760 (1996).
17. A. Bolshakov, W. C. Oliver, and G. M. Pharr, in *Thin Films: Stresses and Mechanical Properties VI,* edited by W. W. Gerberich, H. Gao, J-E. Sundgren, and S. P. Baker (Mater. Res. Soc. Symp. Proc. **436**, Pittsburgh, PA, 1997), p. 760.
18. A. Bolshakov and G. M. Pharr, J. Mater. Res. **13**, 1049 (1998).
19. R. B. King, Int. J. Solids Struct. **23**, 1657 (1987).
20. H. Gao, C-H. Chiu, and J. Lee, Int. J. Solids Struct. **29**, 2471 (1992).
21. D. Stone, W. R. LaFontaine, P. Alexopoulos, T. W. Wu, and C-Y. Li, J. Mater. Res. **3**, 141 (1988).
22. T. Y. Tsui, Ph.D. Dissertation, Rice University, July 1996.
23. D. Tabor, *The Hardness of Metals* (Oxford University Press, London, 1951).
24. A. F. Bower, N. Fleck, A. Needleman, and N. Ogbonna, Proc. R. Soc. Lond. A **441**, 97 (1993).
25. G. M. Pharr, A. Bolshakov, T. Y. Tsui, and J. C. Hay, Mater. Res. Soc. Symp. Proc., in press.